1 2	Evidence for Ambient Dark Aqueous SOA Formation in the Po Valley, Italy
3	
4 5 6 7 8	Amy P. Sullivan <sup>1</sup> , Natasha Hodas <sup>2</sup> , Barbara J. Turpin <sup>3</sup> , Kate Skog <sup>4</sup> , Frank N. Keutsch <sup>4,5</sup> , Stefania Gilardoni <sup>6</sup> , Marco Paglione <sup>6</sup> , Matteo Rinaldi <sup>6</sup> , Stefano Decesari <sup>6</sup> , Maria Cristina Facchini <sup>6</sup> , Laurent Poulain <sup>7</sup> , Hartmut Herrmann <sup>7</sup> , Alfred Wiedensohler <sup>7</sup> , Eiko Nemitz <sup>8</sup> , Marsailidh M. Twigg <sup>8</sup> , and Jeffrey L. Collett, Jr. <sup>1</sup>
9 10	
11	
12	<sup>1</sup> Colorado State University, Department of Atmospheric Science, Fort Collins, Colorado 80523,
13	USA
14 15	<sup>2</sup> California Institute of Technology, Division of Chemical Engineering, Pasadena, California 91125, USA
16 17	<sup>3</sup> Rutgers University, Department of Environmental Sciences, New Brunswick, New Jersey 08901, USA
18	<sup>4</sup> University of Wisconsin – Madison, Department of Chemistry, Madison, Wisconsin 53706,
19	USA
20	<sup>5</sup> Harvard University, Department of Chemistry and Chemical Biology, Cambridge,
21	Massachusetts 02138, USA
22	<sup>6</sup> Istituto di Scienze dell'Atmosfera e del Clima, Consiglio Nazionale delle Ricerche, 40129
23	Bologna, Italy
24	<sup>7</sup> Leibniz Institute for Tropospheric Research, 04318 Leipzig, Germany <sup>8</sup> Centre for Ecology and Hydrology, Bush Estate, Penicuik, EH26QB, United Kingdom
25 26	Centre for Ecology and Hydrology, busin Estate, Peniculk, EH20QB, United Kingdom
27	
28	
29	
30	
31	
32	
33	
34	
35	
36	
37	
38	
39	
40 41	
41	
43	
44	
45	

#### **Abstract**

46 47

48 49

50

51

52 53

54

55

56

57

58

59

60

61 62

63

64

65

66

67

68

69

70

71

72

73 74

75

76 77

Laboratory experiments suggest that water-soluble products from the gas-phase oxidation of volatile organic compounds can partition into atmospheric waters where they are further oxidized to form low volatility products, providing an alternative route for oxidation in addition to further oxidation in the gas-phase. These products can remain in the particle phase after water evaporation forming what is termed as aqueous secondary organic aerosol (aqSOA). However, few studies have attempted to observe ambient agSOA. Therefore, a suite of measurements, including near real-time WSOC (water-soluble organic carbon), inorganic anions/cations, organic acids, and gas-phase glyoxal, were made during the PEGASOS (Pan-European Gas-AeroSols-climate interaction Study) 2012 campaign in the Po Valley, Italy to search for evidence of agSOA. Our analysis focused on four periods: Period A on 19-21 June, Period B on 30 June, 1-2 July, Period C on 3-5 July, and Period D on 6-7 July to represent the first (Period A) and second (Periods B, C, and D) halves of the study. These periods were picked to cover varying levels of WSOC and aerosol liquid water. Plus back trajectory analysis suggested all sites sampled similar air masses on a given day. The data collected during both periods were divided into times of increasing relative humidity (RH) and decreasing RH with the aim of diminishing the influence of dilution and mixing on SOA concentrations and other measured variables. Evidence for local agSOA formation was only observed during Period A. When this occurred, there was a correlation of WSOC with organic aerosol ( $R^2 = 0.84$ ), aerosol liquid water ( $R^2 = 0.84$ ), 0.65), RH ( $R^2 = 0.39$ ), and aerosol nitrate ( $R^2 = 0.66$ ). Additionally, this was only observed during times of increasing RH, which coincided with dark conditions. Comparisons of WSOC with oxygenated organic aerosol (OOA) factors determined from application of positive matrix factorization analysis on the aerosol mass spectrometer observations of the submicron nonrefractory organic particle composition suggested that the WSOC differed in the two halves of the study (Period A WSOC vs. OOA-2  $R^2 = 0.83$  and OOA-4  $R^2 = 0.04$  whereas Period C WSOC vs. OOA-2  $R^2$ = 0.03 and OOA-4  $R^2$  = 0.64). OOA-2 had a high O/C (oxygen/carbon) ratio of 0.77, providing evidence that aqueous processing was occurring during Period A. Key factors for local agSOA production during Period A appear to include: air mass stagnation, which allows aqSOA precursors to accumulate in the region; the formation of substantial local particulate nitrate during the overnight hours, which enhances water uptake by the aerosol; and the presence of significant amounts of ammonia, which may contribute to ammonium nitrate formation and subsequent water uptake and/or play a more direct role in the agSOA chemistry.

#### 1. Introduction

The formation of secondary organic aerosol (SOA) remains a major source of uncertainty in predicting organic aerosol concentrations and properties that affect visibility, health, and climate [Kanakidou et al., 2005]. SOA can form through gas-to-particle partitioning of semi-volatile organic compounds formed from gas-phase oxidation of VOCs (volatile organic compounds) [Seinfeld and Pankow, 2003]. However, laboratory experiments and predictions suggest that water-soluble products from the gas-phase oxidation of VOCs can also partition into atmospheric waters (i.e., clouds, fogs, and aerosol water) and react to form low volatility products. These products can remain in the particle phase after water evaporation, forming what is termed aqueous secondary organic aerosol (aqSOA) (e.g. [Blando et al., 2000; Altieri et al., 2006; Carlton et al., 2007; de Haan et al., 2009; Galloway et al., 2009; Ervens and Volkamer, 2010; Sun et al., 2010; Lee et al., 2012; Monges et al., 2012; Nguyen et al., 2012; Tan et al., 2012; Gaston et al., 2014]).

Evidence that aqSOA may be a contributor to ambient SOA includes a gap between observed SOA and SOA predicted by models that only include SOA formed via gas-phase oxidation and gas-particle partitioning [de Gouw et al., 2005; Heald et al., 2005]. In addition, there is a tendency for smog chamber experiments (generally conducted under dry conditions) to form SOA that is less oxygenated and hygroscopic than ambient SOA, suggesting a missing source of SOA [Aiken et al., 2008]. In some locations, SOA surrogates have been shown to be more strongly correlated with liquid water than organic aerosol [Hennigan et al., 2008; Zhang et al., 2012], contrary to partitioning theory. Lastly, the abundance of ambient oxalate, an important product of aqSOA mechanisms [Carlton et al., 2007; Ervens et al., 2011], cannot be explained solely by gas-phase chemistry.

While it is important to study aqSOA, there have been few studies designed to observe aqSOA formation in the ambient atmosphere. Therefore, a suite of near real-time measurements was assembled with the goal of identifying evidence of aqSOA formation in the Po Valley of Italy during the summer of 2012. A key measurement for this analysis was water-soluble organic carbon (WSOC), which previous research has suggested is a good proxy for SOA (e.g., [Sullivan et al., 2004; Miyazaki et al., 2006; Kondo et al., 2007]). Fog measurements in the Po Valley have been well documented (e.g., [Facchini et al., 1999; Fuzzi et al., 2002]). Fog is unlikely to occur in the summer. But even in summer, the region does have high relative humidity (60% to 80%) and is polluted, providing favorable conditions for aqSOA formation in wet aerosols.

Herein, we present an approach for the investigation of aqSOA formation in the ambient atmosphere and provide results from such analyses. We examine WSOC as a function of known parameters likely to be associated with aqSOA, such as relative humidity (RH), aerosol liquid water (ALW), and organic aerosol (OA) concentration. We also look at the relationship of oxalate with sulfate and gas-phase glyoxal; oxalate and sulfate are both produced by cloud processing and glyoxal is a known precursor to aqSOA formation [Yu et al., 2005; Tan et al., 2009; Ervens and Volkamer, 2010; Lim et al., 2010; Sorooshian et al., 2010]. This study aims to identify conditions conducive to aqSOA formation in this region.

#### 2. Methods

Measurements were conducted within the Italian field campaign of the European Project PEGASOS (Pan-European Gas-AeroSOls-climate interaction Study) in June and July 2012,

focusing on the Po Valley. PEGASOS was a European wide study to address regional to global feedbacks between atmospheric chemistry and climate in different locations as well as in the laboratory. The observations included airborne measurements using a Zeppelin and multiple ground sites to study surface-atmosphere exchange, assess the vertical structure of the atmosphere, and study boundary layer photochemistry. An auxiliary site was located in Bologna. Our measurements were made at the main ground site in San Pietro Capofiume (SPC, Fig. 1 and 2). The SPC field station is located approximately 40 km northeast of Bologna and 30 km south of the Po River in flat terrain of agricultural fields (Fig. 1).

Our measurements included running a Particle-into-Liquid Sampler – Ion Chromatography (PILS-IC) [Orsini et al., 2003] system for inorganic cations, inorganic anions, and light organic acids and a Particle-into-Liquid Sampler – Total Organic Carbon (PILS-TOC) system [Sullivan et al., 2004] for particle-phase WSOC. A PILS collects the ambient particles into purified water, providing the liquid sample for analysis. Both systems operated at 15 LPM with a 2.5 µm size-cut cyclone. Two annular denuders coated with sodium carbonate and phosphorous acid to remove inorganic gases were placed upstream of the PILS-IC and for the PILS-TOC an upstream activated carbon parallel plate denuder [Eatough et al., 1993] was used to remove organic gases. In addition, for the PILS-TOC, a normally open actuated valve controlled by an external timer was periodically closed every 2 hours for 30 min forcing the airflow through a Teflon filter before entering the PILS. This was to allow for a real background measurement to be determined. Ambient PM<sub>2.5</sub> WSOC concentrations were calculated as the difference between the filtered and non-filtered measurements. The background was assumed to be constant between consecutive background measurements. Based on comparison with integrated quartz filter WSOC measurements, it appears the difference between filtered and nonfiltered measurements was being overestimated by ~20% before the carbon denuder was switched out on June 25. Therefore, the WSOC concentrations before this date have been corrected for this.

For the PILS-IC, the liquid sample from the PILS was split between two Dionex ICS-1500 ion chromatographs. These systems include an isocratic pump, self-regenerating anion or cation SRS-ULTRA suppressor, and conductivity detector. The cations were separated using a Dionex IonPac CS12A analytical (4 x250 mm) column with eluent of 18 mM methanesulfonic acid at a flowrate of 1.0 ml/min. A Dionex IonPac AS15 analytical (4 x 250 mm) column employing an eluent of 38 mM sodium hydroxide at a flowrate of 1.5 ml/min was used for the anion analysis. A new chromatogram was obtained every 30 min with a sample loop fill time of 8 min. The limit of detection (LOD) for the various anions and cations was approximately 0.02 µg/m³. These inorganic PILS data were also used to determine ALW from the Extended Aerosol Inorganics Model (E-AIM, [Wexler and Clegg, 2002]) run in a metastable state. More information on the ALW calculations can be found in *Hodas et al.* [2014].

In the PILS-TOC, the liquid sample obtained from the PILS was pushed through a 0.2 µm PTFE liquid filter by a set of syringe pumps to ensure any insoluble particles were removed. The flow was then directed into a Sievers Model 800 Turbo TOC (Total Organic Carbon) Analyzer. This analyzer works by converting the organic carbon in the liquid sample to carbon dioxide through chemical oxidation involving ammonium persulfate and ultraviolet light. The conductivity of the dissolved carbon dioxide formed is determined. The amount of organic carbon in the liquid sample is proportional to the measured increase in conductivity. The

analyzer was run in on-line mode providing a 6 min integrated measurement of WSOC with a LOD of 0.1  $\mu g$  C/m<sup>3</sup>.

Other measurements presented here include 2.5 min integrated organic aerosol (OA) concentrations determined by a High Resolution - Time-of-Flight Aerosol Mass Spectrometer (HR-ToF-AMS) [Drewnick et al., 2005; DeCarlo et al., 2006; Canagaratna et al., 2007]. Positive matrix factorization (PMF) analysis of the AMS OA data was performed using the Multilinear Engine algorithm (ME-2) [Paatero, 1999] implemented within the toolkit Solution Finder (SoFi) developed by Canonaco et al. [2013]. More details on the AMS ME-2 analysis can be found in the supplement text and Fig. S1-S7. Gas-phase glyoxal was determined by the Madison Laser-Induced Phosphorescence (Mad-LIP) instrument [Huisman et al., 2008] at a time resolution of 51 s, hourly integrated ammonia was determined by a Monitor for AeRosols and Gases (MARGA) [ten Brink et al., 2007] in SPC and 30 min ammonia was determined by AiRRmonia [Erisman et al., 2001] in Bologna, and relative humidity was collected at an 1 min time resolution from a Vaisala weather transmitter WXT510. All data presented throughout is hourly averaged starting at the top of the hour.

#### 3. Results and Discussion

### 3.1. Overview

As previously mentioned, WSOC is key to our analysis, since in the absence of biomass burning (see supplement for more details on the source apportionment of the AMS OA), the main contributor to WSOC has been found to be SOA [Sullivan et al., 2006]. Figure 3 shows the time series for WSOC during the entire study at SPC. Overall, the WSOC concentration was higher in the first half of the study (before 25 June) compared with the second half. The WSOC concentration peaked on 19 June then steadily decreased through 22 June. During this time the concentration ranged from about 1 to 7  $\mu$ g C/m³. During July, the WSOC was relatively constant at around 2  $\mu$ g C/m³.

Therefore, our analysis will focus on comparing these two different halves of the study. Given our interest in examining for evidence of aqSOA we picked four periods with varying levels of WSOC and ALW. We also picked cases with both sites sampling similar air masses on a given day. Period A represents the first half of the study and covers 19-21 June. Period A has elevated WSOC and moderate ALW. As indicated by the difference in the length of the back trajectories [*Draxler and Rolph*, 2013; *Rolph*, 2013] shown in Fig. 2, Period A occurred during the end of a stagnation. Period B (30 June, 1-2 July), Period C (3-5 July), and Period D (6-7 July) represent three different cases in the second half of the study. Period B has moderate ALW, Period C has low ALW, and Period D has the highest ALW observed during the study. As indicated by Fig. 2, all three of these periods represent typical background conditions influenced by regional transport, but with slightly different flow patterns. The flows of Periods A and C are most similar. Due to changes in the WSOC concentrations and a non-consistent flow pattern on a daily basis, no periods between 23-29 June were examined.

Cloud cover, as indicated from satellite measurements, showed that the days preceding Period A were generally cloud free whereas clouds developed west of the ground sites preceding Periods B, C, and D (not shown). The presence of clouds was determined by examining satellite pictures set to the view of Europe at 11:00 LT provided by Sat24 (http://en.sat24.com/en/eu). Also, wet scavenging was not likely important as there was very little precipitation at SPC or west of the site during the entire study period. Only two cases of light rain lasting ~30 min,

which occurred on the afternoons of 23 June and 6 July, were recorded at SPC. Table 1 provides a comparison of the various concentrations and parameters observed during all four periods. With the exception of WSOC mentioned above, only the OA and NO<sub>x</sub> (nitric oxides) concentrations across all of Period A are noticeably elevated compared to Periods B, C, and D.

Each period will be examined in terms of the times when RH increased from 40 to 70% (times of RH increasing) and then when the RH decreased from 70 back to 40% (times of RH decreasing). This was done to try to diminish the influence of dilution and mixing on SOA concentrations and measurements of other key variables, since measurements of a conserved tracer were not available. The idea being that the times of RH increasing would represent a time with a stable nocturnal boundary layer. The switch in regimes on average occurs at 05:00 LT, but varied from 03:00 to 08:00 LT. Therefore, the times of RH increasing primarily occurred in the dark. Table S1 provides a list of the exact times used for the times of RH increasing and decreasing in each period.

We first will compare all four periods to examine for evidence of aqSOA. Then we will provide a further examination of aqueous aerosol tracers and WSOC for the two periods with similar air flow (Periods A and C). Our analysis will largely be based on least square regression correlation analysis to examine the relationship between various species and provide a general approach to examine for evidence of aqSOA. We have chosen to examine R<sup>2</sup> values as opposed to p-values since R<sup>2</sup> values can provide a useful tool for explaining the amount of observed variance in a dependent variable that is explained by variation in an independent variable. p-values merely indicate whether a relationship is statistically significant without information about the amount of variance explained. To help categorize the fraction of variance explained, we consider a high correlation as R<sup>2</sup> values greater than 0.7, a moderate correlation as R<sup>2</sup> values between 0.3 to 0.7, and a low correlation as R<sup>2</sup> values less than 0.3.

## 3.2. Evidence for agSOA

WSOC is shown as a function of RH for the times of RH increasing (Fig. 4a and 4b) and decreasing (Fig. 4c and 4d) during Periods A, B, C, and D. For Periods B, C, and D, WSOC had no relationship with RH. Only during the times of increasing RH did Period A have a relationship of increasing WSOC with RH, consistent with local agSOA formation. This can further be illustrated by examining the correlation of WSOC vs. organic aerosol (OA), aerosol liquid water (ALW), and RH for Periods A, B, C, and D during the times of RH increasing (Fig. 5 and S8). In general, WSOC had a strong relationship with OA, but only Period A additionally had a moderate correlation of the WSOC with both ALW (Period A  $R^2 = 0.65$  vs. Period B  $R^2 =$ 0.15, Period C  $R^2 = 0.29$ , and Period D  $R^2 = 0.01$ ) and RH (Period A  $R^2 = 0.39$  vs. Period B  $R^2 = 0.10$ 0.01, Period C  $R^2 = 0.12$ , and Period D  $R^2 = 0.07$ ). The good correlation between WSOC and ALW is in agreement with a previous smog chamber study that found that ALW is a key determinant of SOA yield [Zhou et al., 2011]. This also supports a recent study that observed ambient aqSOA formation during the nighttime as evident by the increased partitioning of gasphase WSOC to the particle-phase with increasing RH [El-Sayed et al., 2015]. The study by El-Sayed et al. [2015] found the increase in the fraction of total WSOC in the particle phase (F<sub>p</sub>) at the two highest RH levels (70-80%, >80%) to be statistically significant compared to the  $F_p$ values at RH < 60%. The main focus of their work was to investigate if the uptake of gas-phase WSOC to aerosol water occurs through reversible or irreversible pathways. The data suggested the aqSOA was formed irreversibly. We investigate this with our data in section 3.3.2.

Figures 6 and S9 show the correlation of WSOC vs. nitrate, oxalate, and sulfate for the times of RH increasing. Nitrate and WSOC are strongly correlated only during the times of RH increasing for Period A. Early morning nitrate peaks were observed at SPC during the first part of the study, but were absent at the upwind Bologna site (Fig. 7). The occurrence of these peaks overlaps with Period A. (Note, the nitrate event observed on 6 and 7 July during Period D will be discussed in Sect. 3.4.) This additionally suggested that the nitrate formation or the ammonium-nitrate-ammonia-nitric acid equilibrium at SPC was locally controlled since the back trajectory analysis indicated both the SPC and Bologna sites were sampling similar upwind air masses to each other in each period (Fig. 2). Therefore, the correlation with locally formed particulate nitrate suggests local formation of WSOC. (Note, increased nitrate also results in higher ALW at the same RH.) This argues that aqSOA formation was predominately local during Period A.

# 3.3. Further Examination of Oxalate, Sulfate, and WSOC During Periods A and C 3.3.1. Oxalate and Sulfate

To help better understand the potential for aqSOA formation, correlations with oxalate and sulfate can be examined. Oxalate and sulfate are known tracers for aerosol formation through cloud processing [Yu et al., 2005; Sorooshian et al., 2010], although sulfate does also have a substantial, albeit slower, gas-phase formation pathway [Seinfeld and Pandis, 2006]. As shown in Fig. 8a and 8b for Periods A and C, during both the times of RH increasing and decreasing, there is a positive linear relationship between oxalate and sulfate (R<sup>2</sup> ranged from 0.39 to 0.68). The association between oxalate and sulfate but not oxalate and WSOC in Period A suggests that the local aqSOA formed in wet aerosols during Period A has little effect on oxalate. This result supports the supposition that oxalate is not a universal marker for agSOA. This is further illustrated in our data by examining the correlation of oxalate vs. gas-phase glyoxal, a known precursor for aqSOA [Tan et al., 2009; Ervens and Volkamer, 2010; Lim et al., 2010], and ALW (Fig. 8c-f). Laboratory experiments suggest a relationship between oxalate and gas-phase glyoxal when there is in-cloud processing as oligomers have been proposed to be the dominant products from processing in aerosol water when hydroxyl radical concentrations are on the order of 10<sup>-12</sup> M [Lim et al., 2010; Tan et al., 2010]. Oxalate could be produced in aerosol water at lower hydroxyl radical concentrations, such as 10<sup>-13</sup> M, due to insufficient organic radical concentrations for oligomer formation [Lee et al., 2011]. Although the hydroxyl radical concentrations are unknown, there is only a relationship between oxalate and gas-phase glyoxal for Period C during times of RH decreasing ( $R^2 = 0.44$ ), which is when clouds were observed west of the site. In addition, there is no important relationship observed between oxalate and ALW for either period (all  $R^2 < 0.17$ ).

# 3.3.2. WSOC

The above analysis suggests that the majority of the WSOC observed during the first half of the study, as illustrated by Period A, is formed locally via chemistry in aerosol liquid water. Clearly, WSOC in the second half of the measurements appears to be different and to derive from different sources. As illustrated by Period C, the WSOC during this time is likely more regional with contributions from gas-to-particle partitioning and possibly in-cloud aqSOA.

To further explore this idea of different types of WSOC, the WSOC observations were compared to positive matrix factorization (PMF) analysis of the AMS OA data collected at SPC.

Five factors, one HOA (hydrocarbon-like OA) and four OOA (oxygenated OA), were found. The four OOA factors include one semi-volatile type (OOA-1) and three low volatility types (OOA-2, OOA-3, and OOA-4). More details on the AMS ME-2 analysis can be found in the supporting information.

 As shown in Fig. 9, the measured WSOC from the first half of the study is dominated by OOA-2 and the second half by OOA-4. This can be further illustrated by looking at the correlation of WSOC vs. OOA-2 and OOA-4 during the times of RH increasing for Periods A and C (Fig. 10). The WSOC in Period A is most strongly correlated with OOA-2 ( $R^2 = 0.83$ ) and in Period C with OOA-4 ( $R^2 = 0.64$ ).

To estimate how each AMS ME-2 factor contributed to WSOC and what fraction of each factor was water-soluble, a multilinear regression analysis was tentatively performed using the method proposed by *Timonen et al.* [2013]. The results are shown in Table S2 and Fig. 11. This approach seeks to reproduce the total WSOC as a linear combination of the different factors, whilst minimizing the residuals and, unlike in *Timonen et al.* [2013], capping the individual factor contributions at 1 to allow conservation of the carbon mass. The regression analysis was carried out with a zero intercept like in *Timonen et al.* [2013], as well as with a non-zero intercept to account for possible instrumental biases between the AMS and PILS methods. Only the four OOA factors were considered, while HOA was assumed to be completely insoluble. All concentrations are in carbon mass units, which for the AMS factors were derived from organic mass concentrations through factor-specific OM/OC ratios. The results of the regression are reported for the whole PILS measurement period and also for Periods A and C separately.

The results for the whole measurement period indicate that the largest contributions to the WSOC must be attributed to the OOA types which were simply the most abundant (OOA-3 and OOA-4), but the water-soluble fractions as reflected in the regression coefficients were greatest for OOA-2 and OOA-4 in agreement with their high correlation coefficients with WSOC. Interestingly, OOA-2 and OOA-4 are also the factors possessing the highest O/C ratios (0.77 and 0.76, respectively), with respect to the other two (O/C = 0.48 for OOA-1 and 0.36 for OOA-3). Therefore, in this study the factor-specific WSOC fractions seem related to the oxygen contents measured by the AMS.

The multilinear regression analysis performed on the Period A measurements suggests that the largest water-soluble fractions are exhibited by OOA-1 and OOA-2, whose concentrations were observed to increase along with RH and WSOC for all the days in this period of the campaign. Due to the very different absolute average concentrations, the second factor (OOA-2) provided the largest contribution to WSOC, accounting for more than one third of the total water-soluble organic carbon concentration. Interestingly, the diurnal trend of OOA-1 indicated that its partitioning to the aerosol phase was largely reversible, and its concentrations declined steeply in the late morning hours when RH and ALW decreased (Fig. 12a). In the same hours of the day, the OOA-2 concentrations were largely unaffected by RH indicating (a) that OOA-2 mainly accounted for oxidized compounds stable in the aerosol phase and (b) that boundary layer growth is not the reason for the decrease in OOA-1 as this should have affected all factors. OOA-1 and OOA-2 can therefore be hypothesized as two aging stages of aqSOA formation during Period A.

Interestingly, some OOA-2 is also produced in Periods B and D. Although the concentrations levels of OOA-2 observed are similar between Periods A and D, OOA-2 concentrations are much more sustained across the day in Period A. In addition, as illustrated in

the diurnal profiles for these periods (Fig. S10) the OOA-2 follows along more closely with OOA-1, RH, and ALW in Periods B and D, likely due to the differences in meteorology and/or chemistry of these periods compared to Period A. Regardless of these differences the observations all still point to the strong relationship between OOA-1, OOA-2, and ALW.

The results obtained for Period C show again that the greatest coefficients (hence the largest water-soluble fractions) were found for OOA-2 and OOA-4. However, due to its very small concentrations in this period, OOA-2 provided a negligible contribution to WSOC (1%), while OOA-4 was estimated to account for more than half of the WSOC carbon content. The examination of time trends indicates that OOA-4 is mainly a background component of the aerosol, showing no appreciable increase at the time when RH increased for a few hours on the mornings of 5 and 6 July. Similar to Period A, here again the times when RH and ALW were high showed relatively high concentrations of OOA-1 (Fig. 12b), which represented an additional (though small compared to OOA-4) contribution to WSOC. Period C provides a case where significant OOA-1 is formed, but not OOA-2.

Overall, whilst not without uncertainty, the above findings support the idea that two different types of WSOC occurred during these two different periods. They also support the idea that aqueous processing is dominating during the times of RH increasing during Period A and OOA-2 represented the most important component. The high O/C ratio of OOA-2 is expected for SOA formed through aqueous-phase reactions, because precursors are water-soluble and thus have low carbon numbers and high O/C ratios. Average O/C ratios of ~0.7 to 1.1 have been observed in the oligomeric products formed from laboratory experiments involving hydroxyl radical oxidation and/or aqueous photolysis of methylglyoxal, glycolaldehyde, and phenolic compounds [Altieri et al., 2008; Tan et al., 2009; Perri et al., 2010; Sun et al., 2010]. The high O/C ratios observed for the other main WSOC component, OOA-4, which dominates Period B, could be explained by extensive aging of non-aqueous SOA [Lambe et al., 2011]. However, incloud aqueous-phase reactions could have occurred upwind of the Po Valley, as indicated by the occurrence of oxalate and clouds previously discussed. Our measurements are fully consistent, in indicating that OOA-4 was mainly transported to the site and was not a product of the local aqueous-phase heterogeneous chemistry in the Po Valley atmospheric surface layer.

# 3.4. Conditions for local aqSOA

What leads to strong local aqSOA formation during Period A at SPC? High ALW was present throughout the study (Fig. 3b). It was observed that the days with the highest ALW also had the highest aerosol loading in the lowest layers of the atmosphere. However, no other day outside of Period A, except for 23 June, had a relationship of WSOC with RH during the times of RH increasing. This suggests that high ALW or aerosol loading alone are not sufficient for local aqSOA formation.

As previously mentioned, during Period A early morning nitrate peaks were observed only at the SPC ground site and not at the urban site. However, just the presence of high nitrate (above 2  $\mu$ g/m³) does not seem to lead to aqSOA as no relationship of WSOC as a function of RH was observed on 6 and 7 July (Period D) when nitrate in concentrations similar to those of Period A were observed at SPC. Interestingly, the nitrate observed on these days was also observed in Bologna (Fig. 7). The timing of the peak nitrate concentration also differed from Period A; it occurred later in the morning, around 07:00 LT, whereas during Period A nitrate peaked around midnight or 01:00 LT and then again around 07:00 LT. This suggests that the

presence and timing of elevated nitrate, which is a strong determinant of ALW, may be important for local aqSOA production and resulting WSOC aerosol concentrations in this region.

As previously mentioned, an examination of possible gas-phase precursors (e.g., aromatic VOCs and glyoxal, Table 1) shows no noticeable decline in concentration from the first to second half of the measurement period. Therefore, a possible explanation for the difference between Period A and the other periods is meteorology. Period A featured an anticyclonic condition that led to air stagnation; the other periods featured stronger transport and ventilation. Therefore, during Periods B, C, and D intermediate products needed to form appreciable concentrations of aqSOA are less likely to quickly accumulate in the local boundary layer.

It is possible that another key ingredient in the chemistry is ammonia. Recent studies have suggested possible aqSOA formation processes mediated by ammonia and other atmospheric bases [Galloway et al., 2009; Nozière et al., 2009; Ortiz-Montalvo et al., 2014; Yu et al., 2011]. Ammonia is prevalent in the Po Valley due to agricultural activities. During Period A, high ammonia concentrations (greater than  $\sim$ 30 µg/m³) were observed only at SPC (Fig. 13a).

Overall, the data suggest that local aqSOA production during the stagnation of Period A is not due to cloud processing. Our results also suggest that this aqueous chemistry occurs in the dark, which likely provides the favorable low temperatures and high RH for nitrate aerosol and ALW [Hodas et al., 2014]. Based on other measurements at SPC, the stagnation conditions and elevated nitrate around midnight occurred each day from 14 June through 23 June, suggesting that the local aqSOA formation actually commenced five days earlier. When all these conditions were met, each day  $\sim 1~\mu g$  C/m³ of new WSOC (determined as the change in WSOC concentration during the times of RH increasing) can be attributed to this process.

# 4. Summary

Measurements were conducted during the PEGASOS Study in the Po Valley of Italy during June and July 2012 in San Pietro Capofiume (SPC). The goal was to look for evidence of aqSOA in the ambient atmosphere. Measurements included near real-time WSOC (a good proxy for SOA), inorganic anions/cations, and organic acids. The data were analyzed in terms of the times when RH increased from 40 to 70% (times of RH increasing) and then when the RH decreased from 70 back to 40% (times of RH decreasing) in order to diminish influences from dilution and mixing on ambient measurements. The analysis focused on four periods: Period A on 19-21 June, Period B on 30 June, 1-2 July, Period C on 3-5 July, and Period D on 6-7 July.

Evidence for local aqSOA formation in wet aerosols was observed during Period A. When this occurred there was a correlation of WSOC with OA, ALW, RH, and nitrate. Additionally, this was only observed during times of RH increasing, suggesting the aqSOA was formed in the dark. The aqSOA formation is thought to be local because elevated nitrate, the driver for aerosol water, was only observed at the main ground site in SPC even though the auxiliary site in Bologna was sampling similar upwind air masses at the time.

A comparison of Periods A and C suggested Period C differed from Period A. The WSOC during Period C was likely formed regionally. Interestingly, during Period C as well as Period A a correlation was found between oxalate and sulfate. This suggests that oxalate concentrations were not strongly affected by local aqSOA formation. More importantly, it indicates that oxalate is not a good universal marker for aqSOA.

A comparison of WSOC with the AMS PMF OOA factors showed that Period A featured high O/C ratios, consistent with aqSOA formation. However, they also reinforce the conclusion

that the composition of the WSOC differed between the two halves of the study. Periods A and C were dominated by two different OOA factors, OOA-2 (locally produced) and OOA-4 (long-range transported), respectively.

Overall, by examining the conditions observed in Period A, the data suggest that the local aqSOA formation observed is not due to cloud processing and occurs in the dark. The timing of elevated nitrate concentrations is critical (around midnight local time) to provide the liquid water reservoir needed for aqueous chemistry. Approximately 1  $\mu g$  C/m³ of new WSOC was formed through this process each day these conditions were met, indicating the importance of aqSOA as a source of ambient OA in this region.

# Acknowledgements

We acknowledge funding from the National Science Foundation under Projects AGS-1050052, AGS-1052611, and AGS-1051338. Measurements at SPC were also funded by the European Union FP7 project PEGASOS (FP7-ENV-2010/265148) and by the Regione Emilia Romagna (project SUPERSITO DRG n. 428/10). The authors thank the European Union FP7 ÉCLAIRE (FP7-ENV-2011/282910) project for funding the ammonia measurements in Bologna, the Energy Research Centre of the Netherlands (ECN) for providing the MARGA instrument at SPC, and C. DiMarco, M. Blom, S. Leeson, T. Hutchings, C. Braban, and L. Giulianelli for supporting the ammonia measurements. The authors gratefully acknowledge the NOAA Air Resources Laboratory (ARL) for the provision of the HYSPLIT transport and dispersion model and/or READY website (http://www.arl.noaa.gov/ready.html) used in this publication.

#### References

Aiken, A.C., DeCarlo, P.F., Kroll, J.H., Worsnop, D.R., Huffman, J.A., Docherty, K.S., Ulbrich,
 I.M., Mohr, C., Kimmel, J.R., Sueper, D., Sun, Y., Zhang, Q., Trimborn, A., Northway,
 M., Ziemann, P.J., Canagaratna, M.R., Onasch, T.B., Alfarra, M.R., Prévôt, A.S.,
 Dommen, J., Duplissy, J., Metzger, A., Baltensperger, U., and Jimenez, J.L.: O/C and
 OM/OC ratios of primary, secondary, and ambient organic aerosols with high-resolution
 time-of-flight aerosol mass spectrometry, *Environ. Sci. Technol.*, 42, 4478-4485, 2008.

502

495

Altieri, K.E., A.G. Carlton, H.-J. Lim, B.J. Turpin, and S.P. Seitzinger, Evidence for oligomer formation in clouds: Reactions of isoprene oxidation products, *Environ. Sci. Technol.*, 40, 4956-4960, 2006.

506 507

508

509

Altieri, K., S.P. Seitzinger, A.G. Carlton, B.J. Turpin, G.C. Klein, and A.G. Marshall, Oligomers formed through in-cloud methylglyoxal reactions: Chemical composition, properties, and mechanisms investigated by ultra-high resolution FT-ICR Mass Spectrometry, *Atmos. Environ*, 42, 1476-1490, 2008.

510 511

Blando, J.D. and B.J. Turpin, Secondary Organic Aerosol Formation in Cloud and Fog Droplets:
 A Literature Evaluation of Plausibility, *Atmos. Environ.*, *34*, 1623-1632, 2000.

514

Canagaratna, M.R., J.T. Jayne, J.L. Jimenez, J.D. Allan, M.R. Alfarra, Q. Zhang, T.B. Onasch, F.
 Drewnick, H. Coe, A. Middlebrook, A. Delia, L.R. Williams, A.M. Trimborn, M.J.
 Northway, P.F. DeCarlo, C.E. Kolb, P. Davidovits, and D.R. Worsnop, Chemical and
 Microphysical Characterization of Ambient Aerosols with the Aerodyne Aerosol Mass
 Spectrometer, *Mass Spectrometry Reviews*, 26, 185-222, 2007.

520

Canonaco, F., M. Crippa, J.G. Slowik, U. Baltensperger, and A.S.H. Prévôt, SoFi, an Igor-based interface for the efficient use of the generalized multilinear engine (ME-2) for the source apportionment: ME-2 application to aerosol mass spectrometer data, *Atmos. Meas. Tech.*, 6, 3649-3661, doi:10.5194/amt-6-3649-2013, 2013.

525

Carlton, A.G., B.J. Turpin, K.E. Altieri, A. Reff, S. Seitzinger, H. Lim, and B. Ervens,
 Atmospheric oxalic acid and SOA production from glyoxal: Results of aqueous
 photooxidation experiments, *Atmos. Environ.*, 41, 7588-7602, 2007.

529

DeCarlo, P.F., J.R. Kimmel, A. Trimborn, M.J. Northway, J.T. Jayne, A.C. Aiken, M. Gonin, K.
 Fuhrer, T. Horvath, K.S. Docherty, D.R. Worsnop, and J.L. Jimenez, Field-Deployable,
 High-Resolution, Time-of-Flight Aerosol Mass Spectrometer, *Anal. Chem.*, 78, 8281-8289, 2006.

534

de Gouw, J.A., Middlebrook, A.M., Warneke, C., Goldan, P.D., Kuster, W.C., Roberts, J.M., Fehsenfeld, F.C., Worsnop, D.R., Canagaratna, M.R., Pszenny, A.A.P., Keene, W.C., Marchewka, M., Bertman, S.B., and Bates, T.S.: Budget of organic carbon in a polluted atmosphere: Results from the New England Air Quality Study in 2002, *J. Geophys. Res.*, 110, D16305, doi:10.1029/2004JD005623, 2005.

de Haan, D.O., A.L. Corrigan, M.A. Tolbert, J.L. Jimenez, S.E. Wood, and J.J. Turley, Secondary organic aerosol formation by self-reaction of methylglyoxal and glyoxal in evaporating droplets, *Environ. Sci. Technol.*, *43*, 8184-8190, 2009.

Draxler, R.R. and G.D. Rolph, HYSPLIT (HYbrid Single-Particle Lagrangian Integrated Trajectory) Model access via NOAA ARL READY Website, available at: http://www.arl.noaa.gov/ready/hysplit4.html (last access: 5 August 2013), NOAA Air Resources Laboratory, Silver Spring, MD, 2013.

Drewnick, F., S.S. Hings, P. DeCarlo, J.T. Jayne, M. Gonin, K. Fuhrer, S. Weimer, J.L. Jimenez,
 K.L. Demerjian, S. Borrmann, and D.R. Worsnop, A New Time-of-Flight Aerosol Mass
 Spectrometer (TOF-AMS) – Instrument Description and First Field Deployment, *Aerosol Sci. Technol.*, 39, 637-658, 2005.

Eatough, D.J., A. Wadsworth, D.A. Eatough, J.W. Crawford, L.D. Hansen, and E.A. Lewis, A multiple system, multi-channel diffusion denuder sampler for the determination of fine-particulate organic material in the atmosphere, *Atmos. Environ. A-Gen.*, *27*, 1213-1219, 1993.

El-Sayed, M.M.H., Y. Wang, and C.J. Hennigan, Direct atmospheric evidence for the irreversible formation of aqueous secondary organic aerosol, *Geophys. Res. Lett.*, 42, doi:10.1002/2015GL064556, 2015.

Ersiman, J.W., R. Otjes, A. Hensen, P. Jongejan, P. van den Bulk, A. Khlystov, H. Möls, and S. Slanina, Instrument development and application in studies and monitoring of ambient ammonia, *Atmos. Environ.*, *35*, 1913-1922, 2001.

Ervens, B., B.J. Turpin, and R.J. Weber, Secondary organic aerosol formation in cloud droplets and aqueous particles (aqSOA): a review of laboratory, field and model studies, *Atmos. Chem. Phys.*, 11, 11069-11102, doi:10.5194/acp-11-11069-2011, 2011.

Ervens, B. and R. Volkamer, Glyoxal processing by aerosol multiphase chemistry: towards a kinetic modeling framework of secondary formation in aqueous particles, *Atmos. Chem. Phys.*, 10, 8219-8244, doi:10.5194/acp-10-8219-2010, 2010.

Facchini, M.C., S. Fuzzi, S. Zappoli, A Andracchio, A. Gelencsér, G. Kiss, Z. Krivácsy, E.
 Mészáros, H.C. Hansson, T. Alsberg, and Y. Zebühr, Partitioning of the organic aerosol
 component between fog droplets and interstitial aerosol, *J. Geophys. Res.*, 104, 26821 26832, 1999.

Fuzzi, S., M.C. Facchini, S. Decesari, E. Matta, and M. Mircea, Soluble organic compounds in fog and cloud droplets: What have we learned over the past few years?. *Atmos. Res.*, *64*, 89-98, 2002.

- Galloway, M.M., P.S. Chhabra, A.W.H. Chan, J.D. Surratt, R.C. Flagan, J.H. Seinfeld, and F.N.
   Keutsch, Glyoxal uptake on ammonium sulphate seed aerosol: Reaction products and
   reversibility of uptake under dark and irradiated conditions, *Atmos. Chem. Phys.*, *9*, 3331-3345, 2009.
- Gaston, C.J., T.P. Riedel, Z. Zhang, A. Gold, J.D. Surratt, and J.A. Thornton, Reactive Uptake of
   an Isoprene-Derived Epoxydiol to Submicron Aerosol Particles, *Environ. Sci. Technol.*,
   48, 11178-11186, 2014.

589

593

597

601

607

611

614

618

623

- Heald, C.L., D.J. Jacob, R.J. Park, L.M. Russell, B.J. Huebert, J.H. Seinfeld, H. Liao, and R.J.
   Weber, A large organic aerosol source in the free troposphere missing from current
   models, *Geophys. Res. Lett.*, 32, L18809, doi:10.1029/2005GL023831, 2005.
- Hennigan, C.J., M.H. Bergin, J.E. Dibb, and R.J. Weber, Enhanced secondary organic aerosol
   formation due to water uptake by fine particles, *Geophys. Lett. Res.*, *35*, L18801,
   doi:10.1029/2008GL035046, 2008.
- Hodas, N., A.P. Sullivan, K. Skog, F.N. Keutsch, J.L. Collett, Jr., S. Decesari, M.C. Facchini,
   A.G. Carlton, A. Laaksonen, and B.J. Turpin, Aerosol liquid water driven by
   anthropogenic nitrate: implications for lifetimes of water-soluble organic gases and
   potential for secondary aerosol formation, *Environ. Sci. Technol.*, 48, 11127-11136,
   2014.
- Huisman, A.J., J.R. Hottle, K.L. Coens, J.P. DiGangi, M.M. Galloway, A. Kammrath, and F.N.
   Keutsch, Laser-Induced Phosphorescence for the in Situ Detection of Glyoxal at Part per
   Trillion Mixing Ratios, *Anal. Chem.*, 80, 5884-5891, 2008.
- Kanakidou, M., et al., Organic aerosol and global climate modelling: a review, *Atmos. Chem. Phys.*, *5*, 1053-1123, doi:10.5194/acp-5-1053-2005, 2005.
- Kondo, Y., Y. Miyazaki, N. Takegawa, T. Miyakawa, R.J. Weber, J.L. Jimenez, Q. Zhang, and
   D.R. Worsnop, Oxygenated and water-soluble organic aerosols in Tokyo, *J. Geophys. Res.*, 112, D01203, doi:10.1029/2006JD007056, 2007.
- Lee, A.K.Y., K.L. Hayden, P. Herckes, W.R. Leaitch, J. Liggio A.M. Macdonald, and J.P.D.
   Abbatt, Characterization of aerosol and cloud water at a mountain site during WACS
   2010: Secondary organic aerosol formation through oxidative cloud processing, *Atmos. Chem. Phys.*, 12, 7103-7116, doi:10.5194/acp-12-7103-2012, 2012.
- Lee, A.K.Y., R. Zhao, S.S. Gao, and J.P.D. Abbatt, Aqueous-phase OH Oxidation of Glyoxal:
  Application of a Novel Analytical Approach Employing Aerosol Mass Spectrometry and
  Complementary Off-Line Techniques, *Journal of Physical Chemistry A*, 115, 1051710526, dx.doi.org/10.1021/jp204099g, 2011.

Lim, Y.B., Y. Tan, M.J. Perri, S.P. Seitzinger, and B.J. Turpin, Aqueous Chemistry and its Role in Secondary Organic Aerosol (SOA) Formation, *Atmos. Chem. Phys.*, *10*, 10521-10539, doi:10.5194/acp-10-10521-2010, 2010.

Lambe, A.T., T.B. Onasch, P. Massoli, D.R. Croasdale, J.P. Wright, A.T. Ahern, L.R. Williams, D.R. Worsnop, W.H. Brune, and P. Davidovits, Laboratory studies of the chemical composition and cloud condensation nuclei (CCN) activity of secondary organic aerosol (SOA) and oxidized primary organic aerosol (OPOA), *Atmos. Chem. Phys.*, 11, 8913–8928, 2011.

Miyazaki, Y., Y. Kondo, N. Takegawa, Y. Komazaki, K. Kawamura, M. Mochida, K. Okuzawa,
 and R.J. Weber, Time-resolved measurements of water-soluble organic carbon in Tokyo,
 *J. Geophys. Res.*, 111, D23206, doi:10.1029/2006JD007125, 2006.

Monge, M.E., T. Rosenørn, O. Favez, M. Müller, G. Adler, A.A. Riziq, Y. Rudich, H. Herrmann,
 C. George, and B. D'Anna, Alternative pathway for atmospheric particles growth, *PNAS*,
 109, 6840-6844, doi:10.1073/pnas.1120593109, 2012.

Nguyen, T.B., P.B. Lee, K.M. Updyke, D.L. Bones, J. Laskin, A. Laskin, and S.A. Nizkorodov, Formation of nitrogen- and sulfur-containing light-absorbing compounds accelerated by evaporation of water from secondary organic aerosols, *J. Geophy. Res.*, 117, D01207, doi:10.1029/2011JD016944, 2012.

Nozière, B., P. Dziedzic, and A. Córdova, Products and Kinetics of the Liquid-Phase Reaction of Glyoxal Catalyzed by Ammonium Ions (NH<sub>4</sub><sup>+</sup>), *J. Phys. Chem. A*, *113*, 231-237, 2009.

Orsini, D.A., Y. Ma, A. Sullivan, B. Sierau, K. Baumann, and R.J. Weber, Refinements to the particle-into-liquid sampler (PILS) for ground and airborne measurements of water-soluble aerosol composition, *Atmos. Environ.*, *37*, 1243-1259, 2003.

Ortiz-Montalvo, D.L., S.A.K. Häkkinen, A.N. Schwier, Y.B. Lim, V.F. McNeill, and B.J. Turpin, Ammonium Addition (and Aerosol pH) Has a Dramatic Impact on the Volatility and Yield of Glyoxal Secondary Organic Aerosol, *Environ. Sci. Technol.*, 48, 255-262, 2014.

Paatero, P., The multilinear engine – A table-driven, least squares program for solving multilinear problems, including the n-way parallel factor analysis model, *J. Comput. Graph. Stat.*, 8, 854-888, 1999.

Perri, M.J., Y.B. Lim, S.P. Seitzinger, and B.J. Turpin, Organosulfates from glycolaldehyde in aqueous aerosols and clouds: Laboratory studies, *Atmos. Environ.*, *44*, 2658-2664, 2010.

Rolph, G.D., Real-time Environmental Applications and Display sYstem (READY) Website, available at: http://www.arl.noaa.gov/ready/hysplit4.html (last access; 5 August 2013), NOAA Air Resources Laboratory, Silver Spring, MD, 2013. Seinfeld, J.H. and S.N. Pandis, *Atmospheric Chemistry and Physics: From Air Pollution to Climate Change*, John Wiley, Hoboken, NJ, 2006.

674

677

680

685

691

696

700

704

709

713

- Seinfeld, J.H. and J.F. Pankow, Organic atmospheric particulate material, *Annu. Rev. Phys. Chem.*, *54*, 121-140, 2003.
- Sorooshian, A., S.M. Murphy, S. Hersey, R. Bahreini, H. Jonsson, R.C. Flagan, and J.H. Seinfeld, Constraining the contribution of organic acids and AMS m/z 44 to the organic aerosol budget: On the importance of meteorology, aerosol hygroscopicity, and region, *Geophys. Res. Lett.*, *37*, L21807, doi:10.1029/2010GL044951, 2010.
- Sullivan, A.P., R.E. Peltier, C.A. Brock, J.A. de Gouw, J.S. Holloway, C. Warneke, A.G. Wollny, and R.J. Weber, Airborne measurements of carbonaceous aerosol soluble in water over northeastern United States: Method development and an investigation into water-soluble organic carbon sources, *J. Geophys. Res.*, 111, D23S46, doi:10.1029/2006JD007072, 2006.
- Sullivan, A.P., R.J. Weber, A.L. Clements, J.R. Turner, M.S. Bae, and J.J. Schauer, A method
   for on-line measurement of water-soluble organic carbon in ambient aerosol particles:
   Recent results from an urban site, *Geophys. Res. Lett.*, 31, L13105,
   doi:10.1029/2004GL019681, 2004.
- Sun, Y.L., Q. Zhang, C. Anastasio, and J. Sun, Insights into secondary organic aerosol formed via aqueous-phase reactions of phenolic compounds based on high resolution mass spectrometry, *Atmos. Chem. Phys.*, 10, 4809-4822, doi:10.5194/acp-10-4809-2010, 2010.
- Tan, Y., A.G. Carlton, S.P. Seitzinger, and B.J. Turpin, SOA from Methylglyoxal in Clouds and
   Wet Aerosols: Measurement and Prediction of Key Products, *Atmos. Environ.*, 44, 5218-5226, 2010.
- Tan, Y., Y.B. Lim, K.E. Altieri, S. Seitzinger, and B.J. Turpin, Mechanisms leading to oligomers
   and SOA through aqueous photooxidation: Insights from OH radical oxidation of acetic
   acid and methylglyoxal, *Atmos. Chem. Phys.*, 12, 801-813, doi:10.5194/acp-12-801-2012,
   2012.
- Tan, Y., M.J. Perri, S.P. Seitzinger, and B.J. Turpin, Effects of Precursor Concentration and
   Acidic Sulfate in Aqueous Glyoxal-OH Radical Oxidation and Implications for
   Secondary Organic Aerosol, *Environ. Sci. Technol.*, 43, 8105-8112, 2009.
- ten Brink, H., R. Otjes, P. Jongejan, and S. Slanina, An instrument for semi-continuous monitoring of the size-distribution of nitrate, ammonium, sulphate and chloride in aerosol, *Atmos. Environ.*, *41*, 2768-2779, 2007.
- 718 Timonen, H., S. Carbone, M. Aurela, K. Saarnio, S. Saarikoski, N.L. Ng, M.R. Canagaratna, M.

Kulmala, V.-M. Kerminen, D.R. Worsnop, and R. Hillamo, Characteristics, sources and water-solubility of ambient submicron organic aerosol in springtime in Helsinki, Finland, *J. Aerosol Sci.*, *56*, 61-77, 2013.

Wexler, A.S. and S.L. Clegg, Atmospheric aerosol models for systems including the ions H<sup>+</sup>, NH<sub>4</sub><sup>+</sup>, Na<sup>+</sup>, SO<sub>4</sub><sup>-2</sup>, NO<sub>3</sub><sup>-</sup>, Cl<sup>-</sup>, Br<sup>-</sup>, and H<sub>2</sub>O, *J. Geophys. Res.*, 107, D14, 4207, doi:10.1029/2001JD000451, 2002.

Yu, G., A.R. Bayer, M.M. Galloway, K.J. Korshavn, C.G. Fry, and F.N. Keutsch, Glyoxal in Aqueous Ammonium Sulfate Solutions: Products, Kinetics, and Hydration Effects, *Environ. Sci. Technol.*, *45*, 6336-6342, 2011.

Yu, J.Z., X.H.H. Huang, J. Xu, and M. Hu, When aerosol sulfate goes up, so does oxalate:
 Implications for the formation mechanisms of oxalate, *Environ. Sci. Technol.*, 39, 128-133, 2005.

Zhang, X., J. Liu, E.T. Parker, P.L. Hayes, J.L. Jimenez, J.A. de Gouw, J.H. Flynn, N. Grossberg, B.L. Lefer, and R.J. Weber, On the gas-particle partitioning of soluble organic aerosol in two urban atmospheres with contrasting emissions: 1. Bulk water-soluble organic carbon, *J. Geophys. Res.*, 117, D00V16, doi:10.1029/2012JD017908, 2012.

Zhou, Y., H. Zhang, H.M. Parikh, E.H. Chen, W. Rattanavaraha, E.P. Rosen, W. Wang, and R.M. Kamens, Secondary organic aerosol formation form xylenes and mixtures of toluene and xylenes in an atmospheric urban hydrocarbon mixture: Water and particle seed effects (II), *Atmos. Environ.*, 45, 3882-3890, 2011.

- **Figure Captions**
- Figure 1. Maps created using Google Earth (version 7.1.5.1557) to show the areas surrounding the (a) Bologna and (b) SPC sampling sites.

767

Figure 2. Characteristic 72 h air mass back trajectories for (a) Period A, (b) Period B, (c) Period C, and (d) Period D at the PEGASOS ground sites of Bologna and SPC. All back trajectories are based on the NOAA ARL HYSPLIT trajectory model.

771

Figure 3. Times series of hourly averaged measured (a) WSOC, (b) calculated ALW, (c) RH, and (d) Temperature at SPC. Any gaps in ALW are due to missing PILS-IC data. The dashed vertical lines indicate midnight local time (UTC+2). Periods A, B, C, and D are also indicated.

775

Figure 4. Hourly averaged WSOC as a function of RH for (a) Periods A and C and (b) Periods
B and D during the times of RH increasing and (c) Periods A and C and (d) Periods B and D
during the times of RH decreasing at SPC. The WSOC was binned into 10% RH bands starting
at 40% RH. The error bars represent the standard deviation at each bin. Numbers above or
below points represent the number of data points in each bin.

781

Figure 5. Correlation of hourly averaged WSOC vs. OA for (a) Period A and (b) Period C,
ALW for (c) Period A and (d) Period C, and RH for (e) Period A and (f) Period C at SPC. All
plots are for during the times of RH increasing.

785

Figure 6. Correlation of hourly averaged WSOC vs. nitrate for (a) Period A and (b) Period C, oxalate for (c) Period A and (d) Period C, and sulfate for (e) Period A and (f) Period C at SPC. All plots are for during the times of RH increasing.

789

Figure 7. Times series of hourly averaged AMS nitrate observed at (a) SPC and (b) Bologna.
The dashed vertical lines indicate midnight local time (UTC+2). Periods A, B, C, and D are also indicated.

793 794

**Figure 8.** Correlation of hourly averaged oxalate vs. sulfate for Periods A and C during the times of RH (a) increasing and (b) decreasing, gas-phase glyoxal for Periods A and C during the times of RH (c) increasing and (d) decreasing, and ALW for Periods A and C during the times of RH (e) increasing and (f) decreasing at SPC.

797 798

795

796

Figure 9. Times series of hourly averaged WSOC with AMS ME-2 factors (a) OOA-1, (b) OOA-2, (c) OOA-3, and (d) OOA-4 at SPC. The units for each factor have been converted from μg/m³ to μg C/m³ using their calculated OM/OC ratio (OOA-1 = 1.81, OOA-2 = 2.15, OOA-3 = 2.13, and OOA-4 = 1.62). The dashed vertical lines indicate midnight local time (UTC+2). Periods A, B, C, and D are also indicated.

804

Figure 10. Correlation of hourly averaged WSOC vs. AMS ME-2 factors OOA-1 for (a) Period A and (b) Period C, OOA-2 for (c) Period A and (d) Period C, OOA-3 for (e) Period A and (f) Period C, and OOA-4 for (g) Period A and (h) Period C at SPC. All plots are for during the times of RH increasing.

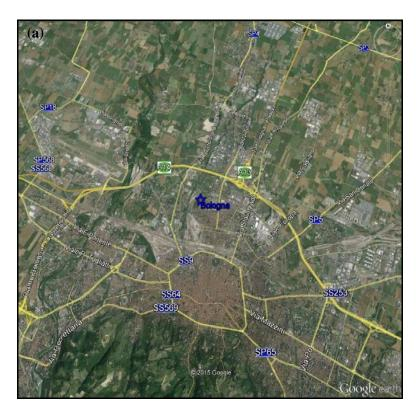
Figure 11. Time series of hourly averaged AMS ME-2 OOA factors, WSOC measured, and WSOC reconstructed for the whole measurement period (top), Period A (bottom left), and Period C (bottom right) at SPC. The units for each OOA factor have been converted from µg/m<sup>3</sup> to µg C/m<sup>3</sup> using their calculated OM/OC ratio. Figure 12. Diurnal profile of WSOC, OOA-1, OOA-2, RH, temperature, ALW, and nitrate for (a) Period A and (b) Period C at SPC. Figure 13. Times series of hourly averaged ammonia observed at (a) SPC and (b) Bologna. The dashed lines indicate midnight local time (UTC+2). Periods A, B, C, and D are also indicated. 

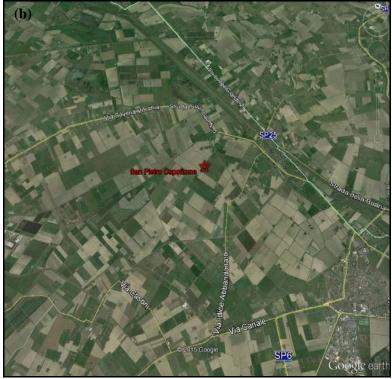
**Table 1.** Average concentrations of aerosol and gas-phase species along with various meteorological parameters observed during the times of RH increasing and decreasing during Periods A, B, C, and D at SPC.

times of Art increasing and decreasing during Ferrous A, B, C, and D at 51 C.															
	OA	WSOC	Glycolate	Acetate	Formate	Chloride	Sulfate	Oxalate	Nitrate	Sodium	Ammonium	Potassium	Magnesium	Calcium	ALW
	$(\mu g/m^3)$	(μg C/m³)	(μg/m <sup>3</sup> )	(μg/m³)	(μg/m <sup>3</sup> )	(μg/m <sup>3</sup> )	(μg/m <sup>3</sup> )	(μg/m³)	(μg/m <sup>3</sup> )	(μg/m <sup>3</sup> )					
Period A	8.93	4.73	0.28	0.40	0.43	0.13	3.49	0.24	2.91	NA	NA	NA	NA	NA	6.81
RH															
Increasing															
Period A	9.63	5.09	0.30	0.33	0.47	0.17	3.23	0.23	5.61	NA	NA	NA	NA	NA	7.29
RH															
Decreasing															
Period B	4.06	2.87	0.22	0.24	0.24	0.09	3.22	0.12	1.67	0.01	1.04	0.43	0.10	0.37	4.21
RH															
Increasing															
Period B	3.78	2.89	0.22	0.24	0.23	0.09	2.69	0.11	1.56	0.01	1.04	0.48	0.09	0.13	4.34
RH															
Decreasing															
Period C	2.05	1.55	0.24	0.28	0.23	0.11	2.80	0.13	1.18	0.04	0.92	0.51	0.11	0.26	2.89
RH															
Increasing															
Period C	2.01	1.54	0.22	0.32	0.23	0.10	2.75	0.12	1.28	0.04	0.94	0.54	0.09	0.06	2.64
RH															
Decreasing															
Period D	2.89	1.92	0.17	0.18	0.21	0.11	3.38	0.12	1.31	0.02	1.07	0.48	0.10	0.32	4.10
RH															
Increasing															
Period D	3.02	1.99	0.19	0.19	0.24	0.14	4.89	0.13	3.56	0.03	2.00	0.55	0.10	0.20	7.90
RH															
Decreasing															

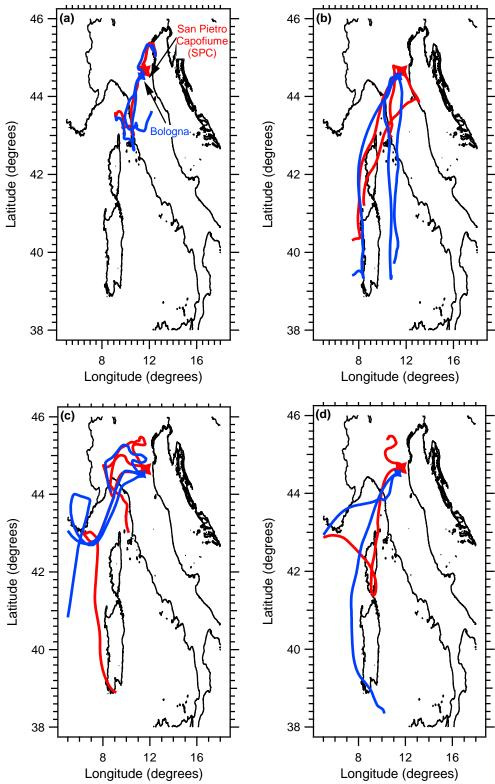
	Ozone (µg/m³)	$NO_x$ $(\mu g/m^3)$	SO <sub>2</sub> (ppb)	Benzene (μg/m³)	Toluene (μg/m³)	Xylene (μg/m³)	Glyoxal (ppb)	T (°C)	RH (%)
Period A RH Increasing	47.42	28.90	0.65	0.21	1.21	0.26	0.05	24.47	64.49
Period A RH Decreasing	63.70	17.75	1.14	0.27	1.78	0.34	0.09	26.09	57.66
Period B RH Increasing	76.6	10.94	0.68	0.19	0.83	0.53	0.06	26.74	60.87
Period B RH Decreasing	51.6	9.30	0.69	0.29	1.43	0.66	0.07	26.2	61.20
Period C RH Increasing	61.29	9.72	0.40	0.17	1.18	0.40	0.05	23.31	60.60
Period C RH Decreasing	75.40	8.08	0.51	0.17	1.11	0.44	0.07	25.02	53.88
Period D RH Increasing	87.21	8.93	0.30	0.12	0.52	0.23	0.05	25.63	63.45
Period D RH Decreasing	93.73	5.12	0.38	0.15	0.85	0.28	0.07	27.32	54.92

Figure 1









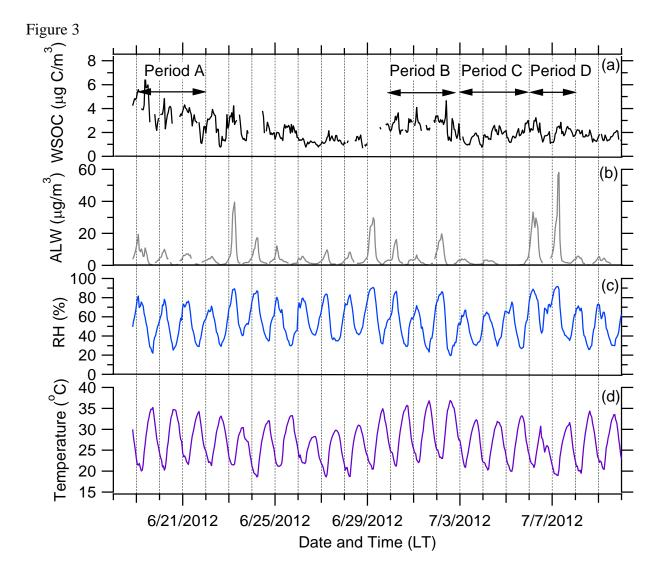


Figure 4

# **RH Increasing**

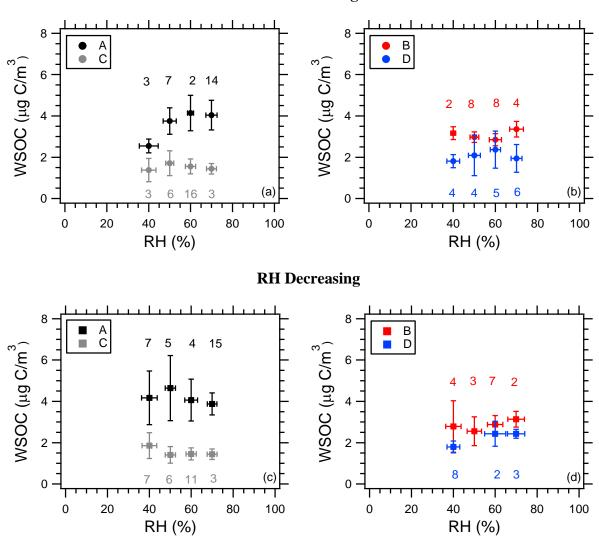


Figure 5

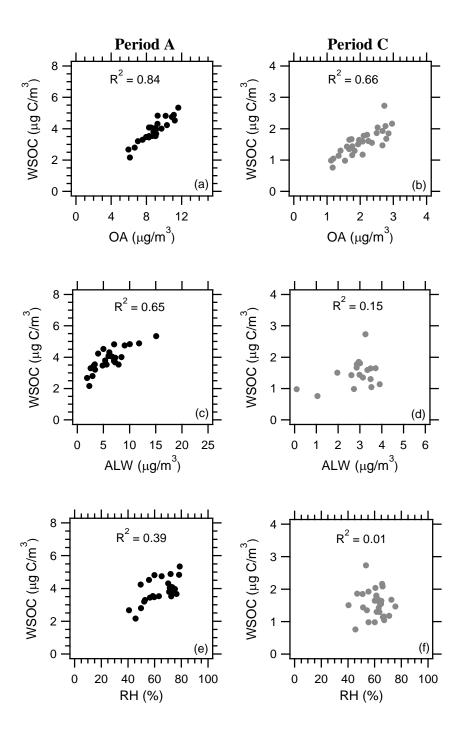
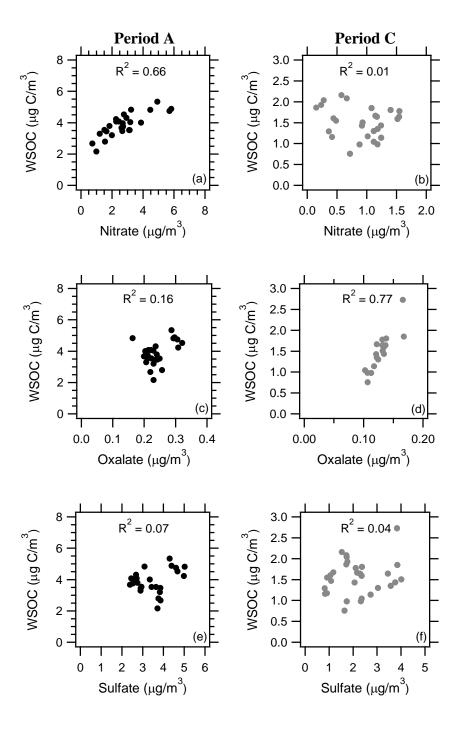


Figure 6





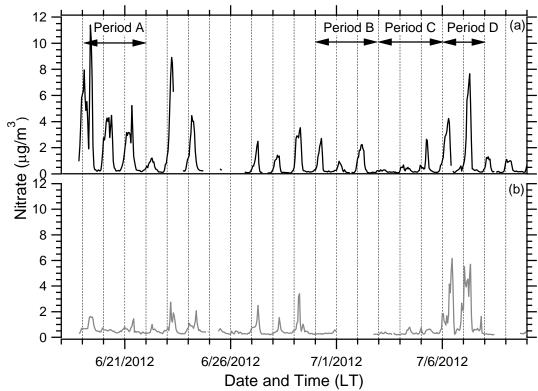


Figure 8

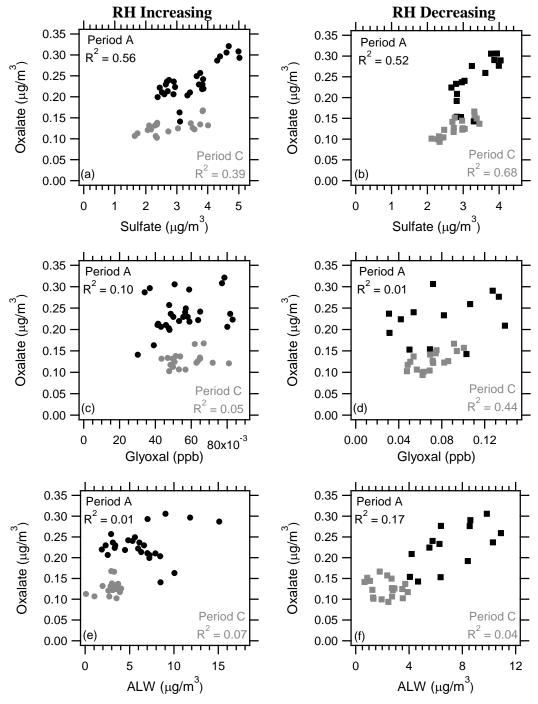
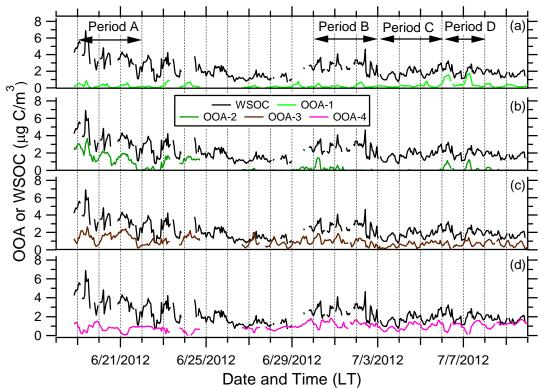
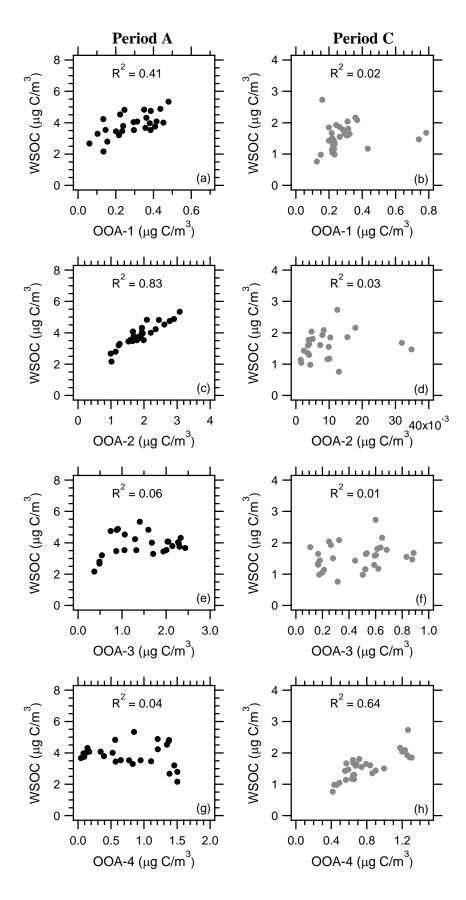


Figure 9





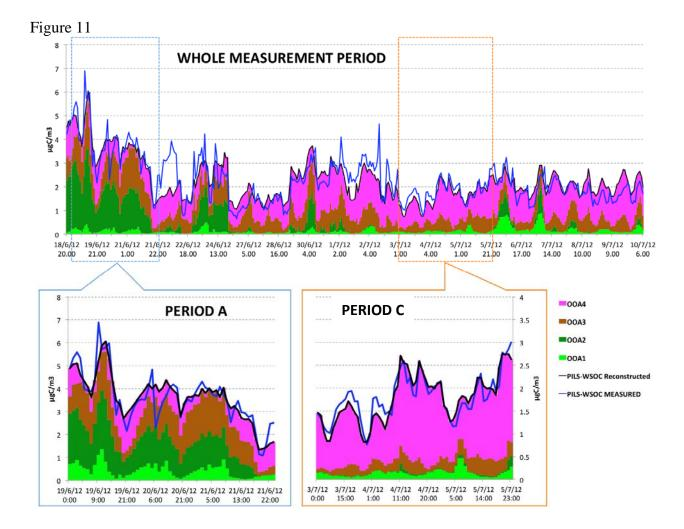


Figure 12

